Int. J. Ion Mobil. Spec. (2013) 16:51–60
DOI 10.1007/s12127-013-0120-x

ORIGINAL RESEARCH

Coupling electrospray corona discharge, charge reduction and ion mobility mass spectrometry: From peptides to large macromolecular protein complexes

Iain D. G. Campuzano · Paul D. Schnier

Received: 6 November 2012 / Revised: 28 December 2012 / Accepted: 15 January 2013 / Published online: 7 February 2013

Abstract We present the design and implementation of a home-built point-to-plane corona discharge probe, which rapidly and efficiently charge reduces biological ions generated by electrospray ionization (ESI). The molecules analysed ranged from small peptides such as Glu-fibrinopeptide B (1.5 kDa), small proteins such as myoglobin (16.9 kDa), polymers such as polyethylene glycol (PEG 10 k) which all showed intense singly charged ions; to large native multiprotein complexes such as GroEL (802 kDa) which show a broad range of charge-reduced species. The corona discharge probe operates at atmospheric pressure and was directly interfaced with a standard-ESI or nanoflow-ESI source of quadrupole ion mobility time-of-flight mass spectrometer. The corona discharge probe is completely modular and could potentially be mounted to any commercial or research grade mass spectrometer with an ESI source. The level of charge reduction is precisely controlled by the applied voltage and/or probe gas flow rate and when in operation, results in approximately a 50 % reduction in total ion current. We also present the combination of corona discharge and travelling wave ion mobility and assign helium collision cross-section values (Ω_{He}) to the charge reduced species of the native protein complex pyruvate kinase. It would appear that the Ω_{He} of the +20 charge state for pyruvate kinase is approximately 20 % smaller than the +35 charge state. Finally, we discuss the potential benefits and concerns of utilising charge reduced protein species as a means of extending the travelling wave collision cross-section calibration range over that which is already published.

Keywords Corona discharge · Electrospray ionization · Travelling wave ion mobility · Peptide · Polyethylene glycol and native protein complex

Introduction

The development and refinement of electrospray [1] (ESI) and nano-electrospray [2] (nESI) ionization allows the user to ionize, and therefore detect by mass spectrometry (MS), an incredibly diverse number of chemical entities, ranging from small organic molecules to peptides [3] and large mega-Dalton viral capsids [4, 5]. ESI and nESI are perceived as a gentle ionization techniques, since it has been demonstrated the preservation of intact protein complexes from solution to gas-phase can be achieved [6]. ESI can also be coupled to liquid chromatographic separation techniques [3] thus increasing its utility. However, above a certain molecular weight, the ions produced by ESI exhibit multiple charging [7–9], therefore in a complex mixture, there could potentially be many over lapping species making data interpretation more challenging. Increased MS-analyser resolution and effective deconvolution algorithms [10] somewhat alleviate this problem. In contrast, matrix assisted laser desorption (MALDI) produces predominantly singly charged ions [11] making it well suited to the analysis of mixtures, especially intact peptides, proteins [12] and polymers [13]. However, in certain instances MALDI has been documented to damage the analyte [14]. The ability to charge-reduce ESI produced ions is of significant benefit, since it combines the utility of ESI and potentially has the ability to produce a simplified spectrum, as observed in MALDI. In the context of ion mobility (IM) and inference of protein structure, the ability to measure the collision cross-section (Ω) of ions which display low charge states can be of significant benefit (*vide infra*).

Electronic supplementary material The online version of this article (doi:10.1007/s12127-013-0120-x) contains supplementary material, which is available to authorized users.

I. D. G. Campuzano (✉) · P. D. Schnier
Department of Molecular Structure and Characterization, Amgen, Thousand Oaks, CA 91320, USA
e-mail: iainc@amgen.com

Charge reduction can be performed using a number of different approaches including ion-ion reactions [15–21], ion-neutral reactions [22, 23] and solution additives [23–25] which have all been utilized to alter the observable charge states of a diverse range of biological ions. Smith and co-workers [15, 16] developed a charge reduction approach in which alpha particles from a ^{210}Po source ionize air in a chamber placed between the ESI capillary and the mass spectrometer inlet. This source could effectively charge-strip protein ions to the singly charged state $[M+H]^+$. In subsequent work, Smith and co-workers replaced the ^{210}Po source with a corona discharge source [18]. We have previously demonstrated that gas-phase ion-neutral charge reduction is an effective method of characterizing heterogeneous polyethylene glycols (PEGs) and PEGylated biomolecules [22]. PEGs and their derivatives are an important biological entity and as such have found wide and varying uses in the biopharmaceutical industry. For example, once PEG forms a bioconjugate with a peptide, protein, lipid or low molecular weight drug molecules [26–29] the circulatory half-life can be increased and importantly, a reduced immunological response can also be observed [30]. Charge stripping can be utilized to decrease the spectral complexity, of PEGylated biomolecules, thus allowing for accurate average molecular weight and molecular weight distributions to be determined. Combining IM and MS and their application in the field of structural biology has proven to be very informative. Initial fundamental protein ion structure research [31, 32] has evolved into topology studies of multiprotein complexes and comparisons to their existing 3-dimensional structures, previously determined by other biophysical techniques. Recent noteworthy examples include membrane proteins [33–35] protein activation [36, 37] substrate binding [38] and optimization of protein networks [39]. The majority of protein charge reduction has been performed on single subunit proteins, and only recently has the benefit of charge reducing noncovalent complexes been demonstrated using ion-neutral atmospheric interactions [23] and solution phase addition of basic compounds [23–25, 36]. The current experimental evidence would suggest that the lowest observable charge state (least amount of charge) of a protein or peptide, is the most native in its conformation or that which most accurately represents the solution state conformation [40–42] by comparison to other biophysical techniques, such as X-ray crystallography and nuclear magnetic resonance [41, 43].

Here we describe the design and implementation of a modular ESI corona discharge probe (CDP) which can rapidly and efficiently charge reduce ionic species, ranging in molecular weight from a small peptide Glu-fibrinopeptide b (GFP; 1.5 kDa) to polyethyleneglycol (PEG; 10 kDa); small denatured proteins such as ubiquitin (UBQ; 8.6 kDa) and large native protein complexes such as alcohol dehydrogenase (ADH; 147.5 kDa), pyruvate kinase (PK; 237 kDa), glutamate dehydrogenase (GDH; 336 kDa) β-galactosidase (β-GAL; 468 kDa) and the tetradecameric chaperone protein complex GroEL (801 kDa). We also examine and discuss travelling wave ion mobility (TWIM) data acquired on the charge reduced native tetrameric complex of pyruvate kinase, for which we have assigned Ω_{He} values.

Experimental

Sample information

The polyethylene glycol sample mPEG2-NHS ester (10 kDa) was dissolved to working concentration of 10 μM in 50 % (v/v) acetonitrile containing 0.1 % (v/v) formic acid. GFP and UBQ were made to working concentrations of 1 μM and 10 μM respectively in 50 %v/v acetonitrile containing 0.1 %v/v formic acid and infused into the MS system at a flow rate of 5 μL/min through the standard ESI source. The proteins ADH; (homotetramer) PK (homotetramer), GDH; (homohexamer) and β-Gal (homotetramer) were used to calibrate the TWIM device and all were dissolved to a stock concentration of 20 μM in water and further buffer exchanged into 100 mM ammonium acetate, using a BioRad P6 spin column. GroEL (homotetradecamer) was prepared as previous described [44]. Working MS solutions of all native protein complexes were 2 μM and infused into the MS system at a flow rate of approximately 10 nL/min using gold coated borosilicate vials via the nESI source. GFP, UBQ, ADH, PK, GDH, β-Gal and GroEL were all purchased from Sigma Aldrich (St. Louis, MO, USA). mPEG2-NHS ester was purchased from NEKTAR (Huntsville, AL, USA). All data processing was performed using MATLAB (The MathWork Inc. Natick, MA) and Igor Pro (WaveMetrics Inc. Lake Oswego, OR).

Corona discharge

The CDP (Fig. 1a & b; Fig. S1, Supporting Information) described within this manuscript was home-built. It consists of an 80 cm PTFE tube, which contains a platinum wire; one end polished/filed into a fine point, contained within an opaque rectangular PEEK housing. This PEEK housing is mounted on to the end of an 8 cm steel tube, which is subsequently mounted on to an x, y, z adjustment stage. A typical point-to-plane distance is 2 mm, which is sufficient to create a strong corona discharge between the end of the platinum wire (point) and the back of the discharge plate (plane). The opposite end of the platinum wire is connected to an external power supply (Stanford Research Systems; Model S355) via a 22 Meg ohm resistor box and gas supply (typically N_2 or medical grade air). The gas supply is "teed-in" to the PTFE tubing which encases the platinum wire,

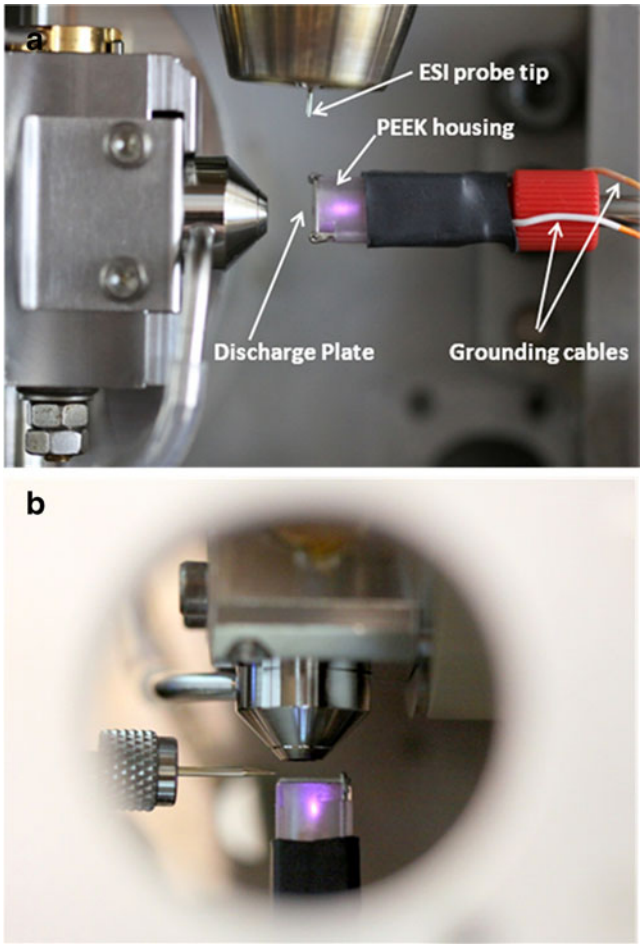

Fig. 1 **a** The corona discharge probe mounted to the standard ESI Z-Spray source of a Synapt HDMS instrument; **b** The corona discharge probe mounted to the nESI Z-Spray source of the same instrument. Note in the nESI image the view is looking down into the source. In both images a corona discharge voltage of −7000 V (470 μA) is being applied

which allows the gas to flow along the platinum wire towards the wire point and the discharge plate orifice. The gas flow rate is controlled by an external flow controller (Dwyer Instruments Inc) and typical flow rates are 10–15 L/min. Typical voltages applied to the CDP are negative 3000 to 7000 V (200 μA to 450 μA). The CDP functions optimally when operated with a relatively high gas flow (10–15 L/min) through the probe, where the gas exits through a small aperture (1.5 mm diameter) in the centre of the steel discharge plate. In our experience it is beneficial to use N_2 as the corona discharge gas, as opposed to medical grade air, which is discussed in more detail in the results section.

Mass spectrometry and travelling wave ion mobility

A Waters Synapt HDMS instrument was used to acquire all MS and TWIM data. The instrument was operated in the positive ionization mode. Typical instrument voltages and pressures were as follows: sample cone 20–50 V (sample dependent); extraction cone 1 V; trap collision energy 3 V; transfer collision energy 2 V, TWIM bias 3 V in ToF mode, 20 V in ToF-TWIM mode; trap-transfer pressure $1.8e^{-3}$ mbar SF_6. To achieve efficient transmission and desolvation of the native protein complexes studied, the source backing pressure was raised to 6.5 mbar. [45, 46] TWIM analysis was performed at a measured pressure of 0.2 mbar N_2 with TWIM velocities of 190, 195 and 200 m/s and a ramped amplitude of 3 to 8 V during each TWIM separation. Three TWIM speeds were chosen to enable the generation of Ω value standard deviations for our measurements. Additionally, Bush and coworkers [47] have established an error of ≤ 3 % for the Ω value of the native complexes, which we use herein to calibrate our TWIM device. All data were acquired over the *m/z* range 600–32,000 (pusher frequency 256 μs) therefore the resulting TWIM separation time is 51.2 ms. Mass scale calibration was carried out using a 50 μg/μL caesium iodide 50 % (v/v) acetonitrile solution. TWIM calibration was undertaken using a group of native protein complexes whose Ω_{He} values were derived on an RF-confining drift-tube instrument, [47] using a well-documented procedure. [46–48] Briefly, the drift-tube Ω_{He} values were adjusted by multiplying by the square root of the reduced mass and dividing by the charge state of the calibrant ions to provide a term that is proportional to the reciprocal mobility of the ion. The measured TWIM arrival-time distributions (ATDs) were corrected for their mass-dependent flight times between the TWIM device and the ToF analyser. The charge and reduced mass corrected Ω_{He} values were plotted against corrected drift-time (ms) values determined using the TWIM separator and the data fitted using an empirically determined polynomial form, $y = ax^2 + bx + c$ [49] (Figure S2, Supporting Information). The derived coefficients are obtained from the calibration curve and used to calculate the Ω_{He} values of the ionic species of interest from their measured TWIM drift-times obtained under identical operating conditions to those of the calibrant species. Published Ω_{He} values for the native protein complexes ADH,[47] PK,[47] GDH,[47] β-Gal [50] and were used for TWIM calibration.

Results & discussion

Corona discharge interfaced to standard-electrospray ionisation

Figure 1a & b show the geometric arrangement of the corona discharge probe interfaced to the Waters Z-Spray source. Figure 2a shows the control ESI mass spectrum of GFP peptide; with the corona discharge probe turned on the charge distribution is shifted to predominantly singly protonated ions. The presumed mechanism of corona discharge are the multiply charged ions (in this case, cations) are reacting with anions

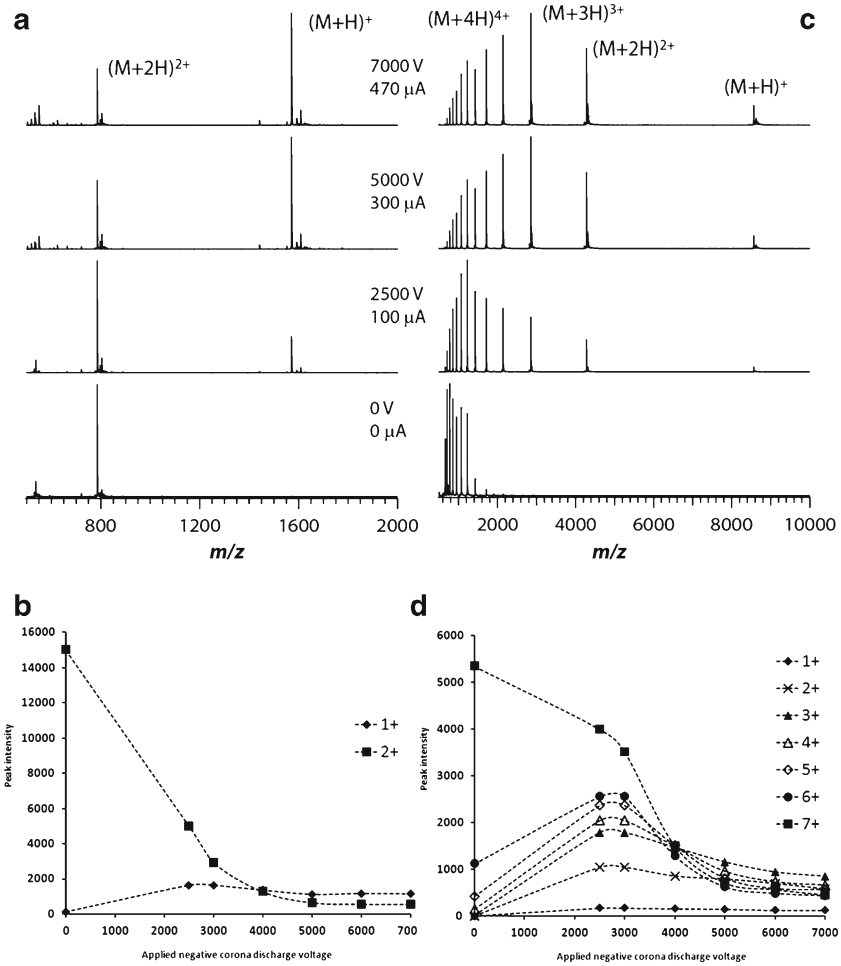

Fig. 2 **a** & **b** Charge reduction profile of Glu-fibrinopeptide **b**; **c** & **d** Charge reduction profile of ubiquitin. The upper figures are selected spectra acquired at different corona discharge voltages (current in μA is also displayed). The lower graphs (**b** & **d**) are the intensity of the individual charge states plotted against the applied corona discharge voltage

generated by the CDP and undergoing proton transfer reactions (*vide infra*). Positioning of the sample probe in both ESI and nESI, in relation to the corona discharge probe is critical. The position for optimal charge reduction appears to be such that the ion beam emitted from the ESI or nESI probe must be directed along the flat surface of the corona discharge plate (Fig. 1a & b). When operated in standard ESI mode, there appears to be no contamination due to the increased analyte flow rate which may result in sample deposition on the PEEK housing. For example, if mPEG2-NHS ester is analysed immediately preceding a protein sample (ESI or nESI), there is no evidence of PEG contamination within the resultant protein spectrum. The lack of contamination can be addressed if one considers the utilized ESI probe flow rate, which in this case is only 5 μL/min. Also the CDP gas flow rate is high (10–15 L/min) which is likely to direct the ESI ion beam away from the CDP, thus minimizing any possible contamination. Additionally and equally important is the positioning of the corona discharge probe in relation to the sample cone. Directing the flow of gas out of the corona discharge probe directly into the sample cone appears to be most effective for charge reduction of the ion under analysis (Fig. 1a & b). The close proximity of the corona discharge probe to the sample cone may suggest that the mixing of the positive and negative ions actually occurs as the flow of gas, containing both the peptide or protein cations and anions (from the corona discharge probe) enter the partial vacuum region of the instrument source. All MS spectra displayed within this manuscript have been acquired using N_2 as the CDP gas. Using medical grade air as the corona discharge gas, instead of N_2, resulted in multiple oxidation modifications to all samples analysed. As can be seen (Figure S3; Supporting Information), when using N_2 there is no significant increase in adduct levels resulting from covalent addition of N_2 molecules to the species if interest. For example if one considers UBQ, multiple covalent additions of 16 and 32 Da can be observed when data are acquired using medical air as the corona discharge gas (Figure S3; Supporting Information).

The level of charge reduction can be easily modulated by either the applied negative discharge voltage or the gas flow (N_2) through the probe. As shown in Fig. 2, when the corona discharge voltage is increased from 0 V (0 μA) to −7000 V (470 μA), the GFP doubly charged ion (*m/z* 785.8) is charge reduced to the singly charged species *m/z* 1570.4 $[M+H]^+$, which now corresponds to the base-peak in the spectrum. If one considers the possibility of charge reduction taking

place by a single electron uptake, analogous to ETD [51] or ECD [52], then the observed charge reduced mass would be *m/z* 1571.4 based on the radical cation species $[M+2H]^{+\bullet}$; this is however not the case (Figure 4, Supporting Information). We would therefore postulate the mechanism of charge reduction is an ion-ion proton transfer reaction, however, the exact mechanism is not yet fully understood. Operating the same corona discharge voltage steps, we have also analysed denatured ubiquitin and at applied corona discharge voltages above −2500 V (100 μA) we observe strong signals for the +1 to +5 charge states. In the absence of a corona discharge, intense signals are observed for the +7 to +13 charge states (Fig. 2c; bottom spectrum). In Fig. 2b & d it is clear that the most intense signals achieved for the +1 charge state, for both GFP and UBQ, are at −2500 to −3000 V. Increasing the corona discharge voltage further, only reduces the intensity of all observable ions during the acquisition. Using the current corona discharge probe design we cannot achieve the same level of charge reduction efficiency observed by Smith and co-workers [18]. Smith and coworkers were able to convert a mixture of small denatured proteins to singly charged ions. This is most likely a kinetic effect, since Smith's design utilized a Faraday cage design and a "line of sight geometry"; the Faraday cage is positioned directly between the ESI probe and the MS inlet nozzle [18] where as the configuration described herein, the ESI probe is positioned orthogonal to the sample cone (MS inlet skimmer) and the CDP. It is likely that the interaction time of the positive and negatively charged ions are longer in Smith's implementation. The primary advantage of our design is that it is completely modular requiring minimal instrument modification and importantly, its utility is demonstrated on a diverse sample set in both ESI and nESI configurations. We are continuing to investigate geometries to improve charge reduction efficiency. As a function of the total ion chromatogram (TIC) there is approximately a 50 % reduction in TIC upon corona discharge application (Figure S5, Supporting Information). This is not surprising, since the MCP detector signal is proportional to charge. Also, as described in Fig. 2b & d, above the optimal applied corona discharge voltage (ca. −3000 V), neutralisation of all ionic species occurs, therefore further reducing the overall ion current. When mPEG2-NHS ester (10K) is electrosprayed from an acetonitrile solution, the resultant mass spectrum is dominated by a complex overlapping series of charge state below *m/z* 2000 (Fig. 3). Once the corona discharge probe is turned on (−7000 V) the complex overlapping ion series below *m/z* 2000 is significantly reduced. Now present are well resolved, intense series representing charges +1, +2, +3, +4 and +5. These spectra compare very favourably to those previously acquired by ion-neutral interaction using the superbases 1,1,3,3-tetramethyl guanidine and 1,8-diazabiclo[5.4.0]-undec-7-ene [22]. The main limitation of the superbase methodology is the difficulty cleaning the instrument after experiments. The neutral superbases can linger for weeks causing all acquired spectra to be charge reduced. In stark contrast, immediately after turning off the corona probe, no charge reduction is observed.

Nano-electrospray ionisation

The corona discharge probe also operates efficiently in combination with the borosilicate nanoflow infusion vials (Fig. 1b). When performing native protein analysis by nESI, it has been demonstrated that the observable charge state with the lowest charge, is more than likely the most native in structure and most likely to represent the solution-phase structure [40–42]. Therefore, being able to rapidly and efficiently reduce the overall charge state of the protein complex of interest is beneficial. Catalina and coworkers [24] have previously demonstrated a range of solution additives termed "proton sponges" to effectively charge reduce a variety of native protein complexes ranging in both molecular weight and stoichiometry. The authors do document reduced signal intensities with additives such as arginine, however, absolute sensitivity reductions are not reported. They also note that solutions containing these "proton sponges" are troublesome for generating a stable nESI spray. The CDP reported herein does not suffer such problems; a reduced TIC of 50 % is observed (Figure S5, Supporting Information) and is considered acceptable and the high flow rate (10–15 L/min) of N_2 gas through the corona discharge probe does not appear to overtly affect nESI sensitivity or the charge state distribution of the native protein complexes. The subsequent work by Van Duijn and coworkers [25] has demonstrated that by the addition of 10 mM imidazole to the protein solution, prior to nESI, effectively reduces the overall charge state distribution of GroEL from +70 (base peak) to +53 (base peak) and interestingly the resultant TWIM ATDs also appear narrower for the ionic species possessing reduced charge, suggesting a lower number of gas-phase conformers. A notable difference between the GroEL data reported herein (Fig. 4d) and that of Van Duijn [25] is that the charge state distribution reported by corona discharge is much broader (+71 to +50; Fig. 4d) than that reported by the addition of imidazole (+58 to +48). Bornschein [23] has recently demonstrated that charge reduction of native protein complexes can also be achieved by cation/neutral interaction by the addition of an unionized basic compound (1,8-diazabicylo[5.4.0]-undec-7-ene) into the nESI source of the mass spectrometer. The data reported herein show a much broader range of charge reduction for the protein complexes ADH (Fig. 4a) and PK (Fig. 5) than that previously reported [23]. Whether such gas-phase protein complex ions possessing significantly reduced charge are representative of solution-phase structures is yet to be determined. Analogous to the ESI probe

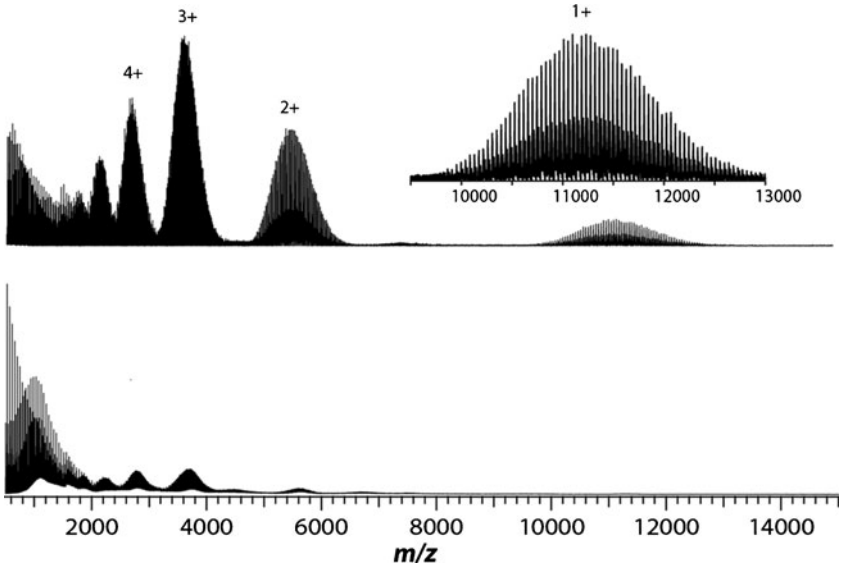

Fig. 3 PEG 10 k analyzed by ESI-corona discharge. Lower spectrum, corona discharge off; upper spectrum, corona discharge on. Inset shows a zoomed-in region of the singly charged PEG 10 k ions. Charge states are also annotated

position, the nESI vial orientation in relation to the corona discharge probe is critical. Spraying along the axis of the discharge plate (Fig. 1b) appears to be the optimal position. Under native buffer and MS conditions (100 mM ammonium acetate) the proteins ADH, GDH, β-Gal and GroEL appear in the *m/z* range 6000, 8000, 10,000 and 12,000 respectively (Fig. 4) with base peak charge states ranging from +25 to +68. Upon corona discharge activation, there is a significant reduction in the overall charge of all native protein complexes. For example, the base peak of β-Gal (Fig. 4b) possesses 44 charges; following charge reduction, the base peak is reduced to 40 charges. However ions can also be observed at *m/z* 18,800 corresponding to the +25 charge state (Table S1, Supporting information). Interestingly, GroEL (Fig. 4d) does not display the same level of charge reduction as the other native complexes investigated. This maybe a function of GroEL's structure, or perhaps native protein complex ions of higher *m/z* value do not undergo the same level of charge reduction as ions of lower *m/z* value. Additionally, what is not currently understood is the observed reduction in charge state distribution towards higher *m/z* values for the native protein MS spectra (Fig. 4a-d) acquired with the corona

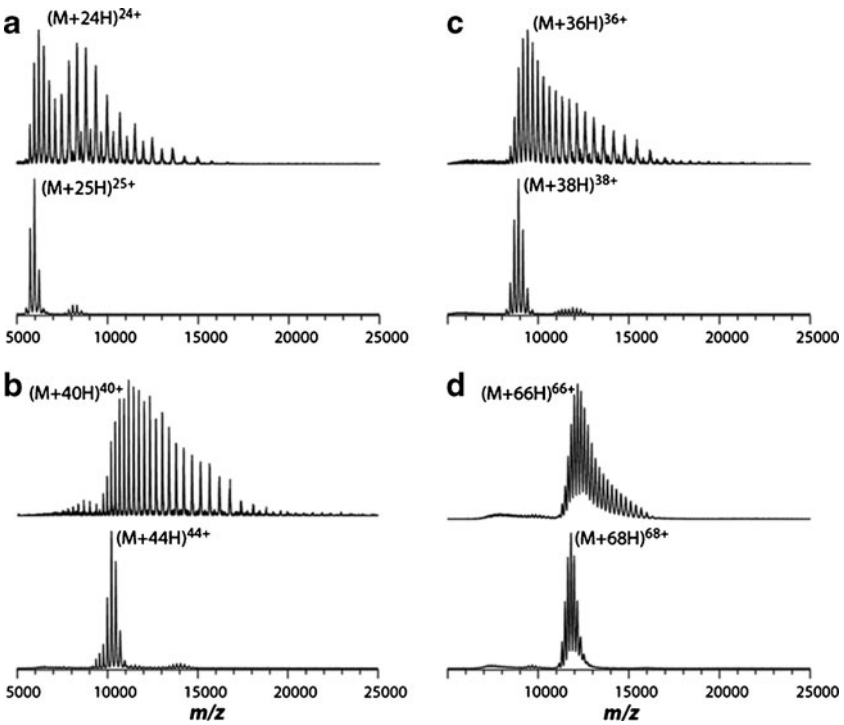

Fig. 4 Native protein complex analysis by nESI-corona discharge; **a** ADH; **b** β-Gal; **c** GDH; **d** GroEL. Lower spectra, corona discharge off; upper spectra, corona discharge on. The most intense (base peak) charge state has been annotated

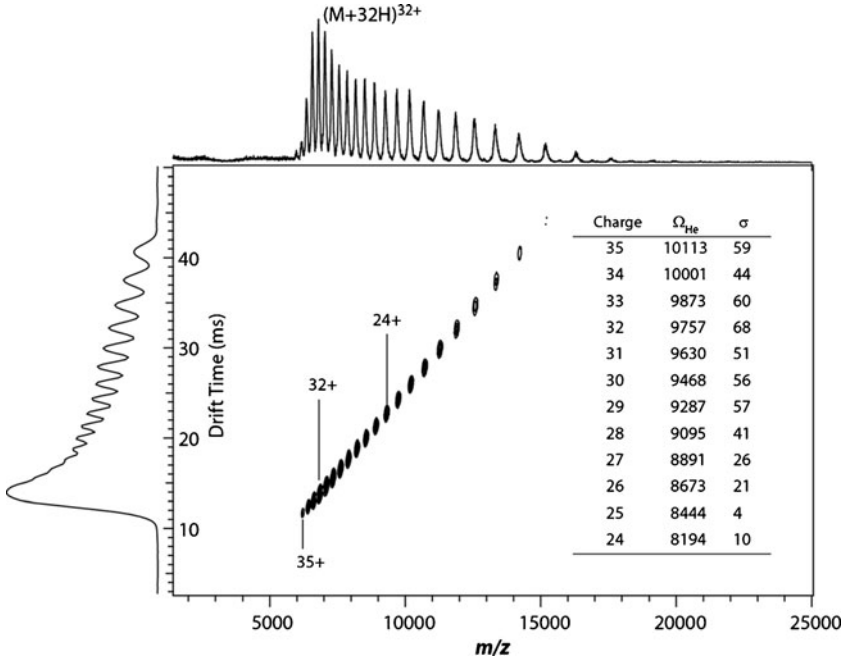

Fig. 5 The native protein complex PK analyzed by nESI-IM corona discharge. Annotated are selected charge states and tabulated Ω_{He} values (Å^2). Standard deviation values (σ) are also reported as Å^2 and were derived from three TWIM measurements made at three different TWIM velocities; 190, 195 and 200 m/s. The data is displayed as an intensity map; the *x*-axis represents the *m/z* scale and the *y*-axis represents the total TWIM drift-time (ms)

discharge source on; are the lower intensity high *m/z* values a result of poor ion transmission through the instrument or inefficient detector response for large molecular weight ions possessing reduced charge? Or are these ions not produced in abundant quantities during the ESI-corona discharge interaction? This is currently under further investigation.

Travelling wave ion mobility

A number of experimental parameters must be carefully considered when performing a TWIM separation of charge reduced species. First, the TWIM amplitude must be ramped during the experiment. This is to ensure that all the observable charge states produced upon charge reduction are well separated over the entire TWIM drift-time function. If one was to use a single TWIM amplitude it would be challenging to achieve such uniform TWIM separation on such large ions with a wide spread of charge and mobility. For example, the observable charge-reduced charge states from the protein PK are +35 to +14 (Fig. 5; Table S2; Figure S6, Supporting Information). Secondly, the TWIM pressure was reduced from the standard operating pressure of 0.5 mbar to 0.2 mbar (N_2). The result of which dramatically improves the overall transmission of the lower charge/high *m/z* ionic species. Another alternative approach to improve ion transmission is to increase the TWIM bias value from the standard 18 V to 40 V. This improves transmission of the lower charge-high *m/z* ionic species, but ion activation becomes a factor, and when analyzing native protein complexes, ion activation [37] must be avoided if one is to derive any native Ω measurements from the TWIM ATDs. Using the proteins ADH, GDH and β-Gal, an effective TWIM calibration (Figure S2, Supporting Information) can be performed over the Ω_{He} range 6830 Å^2 to 15,640 Å^2. These native protein complexes also span a relatively wide *m/z* range; 5800 to 10,000. With this *m/z* range in mind, a TWIM calibration was performed and Ω_{He} values were assigned to the PK charge reduced species which fell within this *m/z* and drift-time range (Fig. 5 & Table S2, Supporting Information). The authors are well aware that ion movement through a TWIM device is complex [53, 54] even when a single TWIM amplitude is utilised, and since all TWIM measurements were performed using a TWIM amplitude ramp (3–8 V), we describe our reported Ω_{He} values as purely tentative (Fig. 5 and Table S2, Supporting Information); only limited structural assignments are inferred *vide infra*. Figure 5 represents a charge reduced TWIM spectrum acquired for the protein PK under native conditions, and considering the measured Ω_{He} values of pyruvate kinase which only fall within the calibration range of ADH, GDH and β-Gal, we can assign tentative Ω_{He} values to charge states +35 to +24. From these values it appears that there is a gradual decrease in Ω_{He} value; 10,113 Å^2 for +35 to 8194 Å^2 for +24 (Fig. 5 & Table S2, Supporting Information). These results suggest that the lower the overall charge of the pyruvate kinase complex, the more compact the structure becomes. Based on previous IM and TWIM observations [47, 48] more accurate Ω value (He and N_2) derivation is achieved when the charge states, molecular weights and Ω values of the calibrant and analyte ions closely match. For example, the charge states of β-Gal (the final TWIM calibration points; Figure S2, Supporting Information) range from +45 to +48, which possess similar TWIM drift-time ranges as the +24 to +28 charge states of

charged-reduced pyruvate kinase. The charge, *m/z* and Ω values of these ions are clearly very different however their mobilites are similar, therefore the extent to which the aforementioned properties may introduce errors into the TWIM derived Ω_{He} values for the measured pyruvate kinase complex is not yet clearly understood.

If one compares the pyruvate kinase charge states which are common to both the native nESI and corona discharge nESI sample, there are some interesting observations which can be made. The TWIM derived Ω_{He} values for the native nESI and corona discharge nESI for charge states +35 through +32 are essentially identical (Figure S7, Table S2 & S3, Supporting Information). For example, the TWIM measured Ω_{He} value for the native (corona discharge off) and corona discharge on, +35 charge state are 10,075 ±7 $Å^2$ and 10,113 ±59 $Å^2$ respectively. The ATD peak shapes are also closely matched. There is also little measureable difference in measured Ω_{He} value for the +32 charge state; 9828 ±58 $Å^2$ (corona discharge off) and 9757 ±68 $Å^2$ (corona discharge on). This would imply that there is little or no measurable structural alteration for a given charge state of a native protein complex (PK) upon ESI corona discharge charge reduction.

One could envisage that if mobility measurements were performed on a drift-tube instrument [47, 48, 55] operating with a nESI corona discharge source, one could obtain Ω measurements in both He and N_2 which could potentially be used as TWIM calibrant species, spanning a wide *m/z* and importantly, wide mobility range. This is currently under investigation, since it is not clear as to whether ions of significantly reduced charge would make suitable TWIM calibrants for ions possessing higher levels of charge. Additionally, one could use this approach to further examine the properties of large biological ions as a function of Ω value and activation energy analogous to those recently published by Hall [36]. Using corona discharge one could access and explore a much broader range of charge states than those currently available though solution [24, 25] and gas-phase [23] charge reduction.

Conclusion

An in-house built probe which operates by producing localized negatively charged ions by the mechanism of point-to-plane corona discharge has been demonstrated on a wide sample class range. This modular design can potentially be fitted to any instrument ESI source. Efficient manipulation of ionic charge can readily be performed by either adjustment of the corona discharge voltage or the gas flow (N_2) through the probe in either ESI or nESI mode, with no significant loss in detection sensitivity. Effective charge reduction has been demonstrated on GFP, UBQ, PEG 10K and the native protein complexes ADH, PK, GDH, β-Gal and GroEL. We have demonstrated that for the protein complex PK, a particular charge state, regardless of whether it was generated by nESI or corona discharge nESI, the measured Ω values were essentially identical. We have also calculated TWIM Ω_{He} values for the charge-reduced charge states (+35 to +24) of the native protein complex PK. Utilizing known protein standards as TWIM calibrants, it appears that the Ω_{He} values of the charge reduced PK complex decreases by 20 % as the charge reduces from +35 to +24. Crucial to detection of these low mobility charge reduced species, are the optimisation of instrument parameters such as TWIM bias, pressure, amplitude. Moreover, the combination of corona discharge charge reduction has the potential to produce a new set of TWIM protein calibration standards that span a wide *m/z*, charge and mobility range. It would appear from the diverse sample set presented herein, this home built corona discharge source can be used as a generic method for ionic charge reduction. This has the distinct advantage of not having to add solution additives or the use of strong basic compounds or radioactive particles in the source of the mass spectrometer to achieve ionic charge reduction. We envisage this simple and rapid method of reducing an ions charge, in particular, native protein complexes will prove very effective for future structural biology IM-MS experiments.

Acknowledgments The authors would like to thank Ed FitzGerald (Amgen) for producing the high quality source photographs displayed in this manuscript. Jeff Brown and Mike Morris (Waters Corporation, MS Technologies Centre, UK) are gratefully acknowledged for their useful discussions during the design and optimization of the electrospray corona discharge probe.

References

1. Fenn JB, Mann M, Meng CK, Wong SF, Whitehouse CM (1989) Electrospray ionization for mass spectrometry of large biomolecules. Science 246(4926):64–71
2. Wilm M, Mann M (1996) Analytical properties of the nanoelectrospray ion source. Anal Chem 68(1):1–8
3. Bier ME, Bruins AP, Chernushevich IV et al (1997) Electrospray ionisation mass spectrometry: fundamentals, instrumentation and applications (Ed Cole RB), Wiley-Interscience Publication, John Wiley & Sons Inc
4. Uetrecht C, Versluis C, Watts NR, Wingfield PT, Steven AC, Heck AJ (2008) Stability and shape of hepatitis B virus capsids in vacuo. Angew Chem Int Ed Engl 47(33):6247–6251. doi:10.1002/anie.200802410
5. Uetrecht C, Versluis C, Watts NR, Roos WH, Wuite GJ, Wingfield PT, Steven AC, Heck AJ (2008) High-resolution mass spectrometry of viral assemblies: molecular composition and stability of dimorphic hepatitis B virus capsids. Proc Natl Acad Sci U S A 105(27):9216–9220. doi:10.1073/pnas.0800406105
6. Loo JA, Holler TP, Foltin SK, McConnell P, Banotai CA, Horne NM, Mueller WT, Stevenson TI, Mack DP (1998) Application of electrospray ionization mass spectrometry for studying human immunodeficiency virus protein complexes. Proteins Suppl 2:28–37

7. Iribarne JV, Thomson BA (1976) On the evaporation of small ions from charged droplets. J Chem Phys 64:2287–2295. doi:10.1063/1.432536
8. Dole M, Mach LL, Hines RL, Mobley RC, Ferguson LP, Alice MB (1968) MOlecular beams of macroions. J Chem Phys 49:2240–2250. doi:10.1063/1.1670391
9. Fenn JB (2003) Electrospray wings for molecular elephants (Nobel lecture). Angew Chem Int Ed Engl 42(33):3871–3894. doi:10.1002/anie.200300605
10. Ferrige AG, Seddon MJ, Green BN, Jarvis SA, Skilling J (1992) Disentangling electrospray spectra with maximum entropy. Rapid Commun Mass Spectrom 6:707–711
11. Karas M, Bachman D, Hillenkamp F (1987) Int J Mass Spectrom Ion Processes 78:53–68
12. Hillenkamp F, Karas M, Beavis RC, Chait BT (1991) Matrix-assisted laser desorption/ionization mass spectrometry of biopolymers. Anal Chem 63(24):1193A–1203A
13. Pasch H, Schrepp WP (2003) MALDI TOF Mass Spectrometry of Synthetic Polymers (Springer Laboratory, Springer-Verlag, Berlin, Heidelberg)
14. Smith RD, Udseth HR, Wahl JH, Goodlett DR, Hofstadler SA (1996) Capillary electrophoresis-mass spectrometry. Methods Enzymol 271:448–486
15. Scalf M, Westphall MS, Krause J, Kaufman SL, Smith LM (1999) Controlling charge states of large ions. Science 283(5399):194–197
16. Scalf M, Westphall MS, Smith LM (2000) Charge reduction electrospray mass spectrometry. Anal Chem 72(1):52–60
17. Smith LM (2008) Is charge reduction in ESI really necessary? J Am Soc Mass Spectrom 19(5):629–631. doi:10.1016/j.jasms.2008.02.002
18. Ebeling DD, Westphall MS, Scalf M, Smith LM (2000) Corona discharge in charge reduction electrospray mass spectrometry. Anal Chem 72(21):5158–5161
19. Pitteri SJ, McLuckey SA (2005) Recent developments in the ion/ion chemistry of high-mass multiply charged ions. Mass Spectrom Rev 24(6):931–958. doi:10.1002/mas.20048
20. Zhao Q, Schieffer GM, Soyk MW, Anderson TJ, Houk RS, Badman ER (2010) Effects of ion/ion proton transfer reactions on conformation of gas-phase cytochrome c ions. J Am Soc Mass Spectrom 21(7):1208–1217. doi:10.1016/j.jasms.2010.03.032
21. Zhao Q, Soyk MW, Schieffer GM, Fuhrer K, Gonin MM, Houk RS, Badman ER (2009) An ion trap-ion mobility-time of flight mass spectrometer with three ion sources for ion/ion reactions. J Am Soc Mass Spectrom 20(8):1549–1561. doi:10.1016/j.jasms.2009.04.014
22. Bagal D, Zhang H, Schnier PD (2008) Gas-phase proton-transfer chemistry coupled with TOF mass spectrometry and ion mobility-MS for the facile analysis of poly(ethylene glycols) and PEGylated polypeptide conjugates. Anal Chem 80(7):2408–2418. doi:10.1021/ac7020163
23. Bornschein RE, Hyung SJ, Ruotolo BT (2011) Ion mobility-mass spectrometry reveals conformational changes in charge reduced multiprotein complexes. J Am Soc Mass Spectrom 22(10):1690–1698. doi:10.1007/s13361-011-0204-y
24. Catalina MI, van den Heuvel RH, van Duijn E, Heck AJ (2005) Decharging of globular proteins and protein complexes in electrospray. Chemistry 11(3):960–968. doi:10.1002/chem.200400395
25. van Duijn E, Barendregt A, Synowsky S, Versluis C, Heck AJ (2009) Chaperonin complexes monitored by ion mobility mass spectrometry. J Am Chem Soc 131(4):1452–1459. doi:10.1021/ja805513410.1021/ja8055134
26. Roberts MJ, Bentley MD, Harris JM (2002) Chemistry for peptide and protein PEGylation. Adv Drug Deliv Rev 54(4):459–476
27. Shi F, Wasungu L, Nomden A, Stuart MC, Polushkin E, Engberts JB, Hoekstra D (2002) Interference of poly(ethylene glycol)-lipid analogues with cationic-lipid-mediated delivery of oligonucleotides; role of lipid exchangeability and non-lamellar transitions. Biochem J 366(Pt 1):333–341. doi:10.1042/BJ20020590BJ20020590
28. Mishra S, Webster P, Davis ME (2004) PEGylation significantly affects cellular uptake and intracellular trafficking of non-viral gene delivery particles. Eur J Cell Biol 83(3):97–111
29. Yu H, Li X, Marchetto GS, Dy R, Hunter D, Calvo B, Dawson TL, Wilm M, Anderegg RJ, Graves LM, Earp HS (1996) Activation of a novel calcium-dependent protein-tyrosine kinase. Correlation with c-Jun N-terminal kinase but not mitogen-activated protein kinase activation. J Biol Chem 271(47):29993–29998
30. Monfardini C, Veronese FM (1998) Stabilization of substances in circulation. Bioconjug Chem 9(4):418–450. doi:10.1021/bc970184fbc970184f
31. Wyttenbach TvH G, Bowers MT (1996) Gas-phase conformation of biological molecules: Bradykinin. J Am Chem Soc 118:8355–8364
32. Clemmer DE, Hudgins RR, Jarrold MF (1995) Naked protein conformations: cytochrome c in the gas phase. J Am Chem Soc 117:10141–10142
33. Borysik AJ, Robinson CV (2012) The 'sticky business' of cleaning gas-phase membrane proteins: a detergent oriented perspective. Phys Chem Chem Phys 14(42):14439–14449. doi:10.1039/c2cp41687e
34. Borysik AJ, Robinson CV (2012) Formation and dissociation processes of gas-phase detergent micelles. Langmuir 28(18):7160–7167. doi:10.1021/la3002866
35. Leney AC, McMorran LM, Radford SE, Ashcroft AE (2012) Amphipathic polymers enable the study of functional membrane proteins in the gas phase. Anal Chem. doi:10.1021/ac302223s
36. Hall Z, Politis A, Bush MF, Smith LJ, Robinson CV (2012) Charge-state dependent compaction and dissociation of protein complexes: insights from ion mobility and molecular dynamics. J Am Chem Soc 134(7):3429–3438. doi:10.1021/ja2096859
37. Ruotolo BT, Hyung SJ, Robinson PM, Giles K, Bateman RH, Robinson CV (2007) Ion mobility-mass spectrometry reveals long-lived, unfolded intermediates in the dissociation of protein complexes. Angew Chem Int Ed Engl 46(42):8001–8004. doi:10.1002/anie.200702161
38. Hopper JT, Rawlings A, Afonso JP, Channing D, Layfield R, Oldham NJ (2012) Evidence for the preservation of native inter- and intra-molecular hydrogen bonds in the desolvated FK-binding protein.FK506 complex produced by electrospray ionization. J Am Soc Mass Spectrom 23(10):1757–1767. doi:10.1007/s13361-012-0430-y
39. Pukala TL, Ruotolo BT, Zhou M, Politis A, Stefanescu R, Leary JA, Robinson CV (2009) Subunit architecture of multiprotein assemblies determined using restraints from gas-phase measurements. Structure 17(9):1235–1243. doi:10.1016/j.str.2009.07.013
40. Ruotolo BT, Giles K, Campuzano I, Sandercock AM, Bateman RH, Robinson CV (2005) Evidence for macromolecular protein rings in the absence of bulk water. Science 310(5754):1658–1661. doi:10.1126/science.1120177
41. Scarff CA, Thalassinos K, Hilton GR, Scrivens JH (2008) Travelling wave ion mobility mass spectrometry studies of protein structure: biological significance and comparison with X-ray crystallography and nuclear magnetic resonance spectroscopy measurements. Rapid Commun Mass Spectrom 22(20):3297–3304. doi:10.1002/rcm.3737
42. Wyttenbach T, Bowers MT (2011) Structural stability from solution to the gas phase: native solution structure of ubiquitin survives analysis in a solvent-free ion mobility-mass spectrometry environment. J Phys Chem B 115(42):12266–12275. doi:10.1021/jp206867a
43. Smith DP, Knapman TW, Campuzano I, Malham RW, Berryman JT, Radford SE, Ashcroft AE (2009) Deciphering drift time

measurements from travelling wave ion mobility spectrometry-mass spectrometry studies. Eur J Mass Spectrom (Chichester, Eng) 15(2):113–130. doi:10.1255/ejms.947
44. Campuzano I, Giles K (2011). Nanoproteomics: Methods and Protocols, Methods in Molecular Biology (Eds: Toms SA, Weil R), Humana Press, a part of Springer Science+Business Media, LLC, New York (790):57–70
45. Tahallah N, Pinkse M, Maier CS, Heck AJ (2001) The effect of the source pressure on the abundance of ions of noncovalent protein assemblies in an electrospray ionization orthogonal time-of-flight instrument. Rapid Commun Mass Spectrom 15(8):596–601. doi:10.1002/rcm.275
46. Ruotolo BT, Benesch JL, Sandercock AM, Hyung SJ, Robinson CV (2008) Ion mobility-mass spectrometry analysis of large protein complexes. Nat Protoc 3(7):1139–1152. doi:10.1038/nprot.2008.78
47. Bush MF, Hall Z, Giles K, Hoyes J, Robinson CV, Ruotolo BT (2010) Collision cross sections of proteins and their complexes: a calibration framework and database for gas-phase structural biology. Anal Chem 82(22):9557–9565. doi:10.1021/ac1022953
48. Salbo R, Bush MF, Naver H, Campuzano I, Robinson CV, Pettersson I, Jorgensen TJ, Haselmann KF (2012) Traveling-wave ion mobility mass spectrometry of protein complexes: accurate calibrated collision cross-sections of human insulin oligomers. Rapid Commun Mass Spectrom 26(10):1181–1193. doi:10.1002/rcm.6211
49. Bush MF, Campuzano IDG, Robinson CV (2012) Ion Mobility Mass Spectrometry of Peptide Ions: Effects of Drift Gas & Calibration Strategies. Anal Chem 84(16):7124–7130. doi:10.1021/ac3014498
50. Bush MF, Hall Z, Politis A, Barsky D, Robinson CV. Interpreting the Collision Cross Sections of Protein Complexes: Models, Approximations, Errors, and Best Practices. Proc. 59th ASMS Conf. Mass Spectrometry and Applied Topics, 2011, WOB.
51. Syka JE, Coon JJ, Schroeder MJ, Shabanowitz J, Hunt DF (2004) Peptide and protein sequence analysis by electron transfer dissociation mass spectrometry. Proc Natl Acad Sci U S A 101(26):9528–9533. doi:10.1073/pnas.0402700101 0104027001 01
52. Zubarev RA, Kelleher NL, McLafferty FW (1998) Electron capture dissociation of multiply charged protein cations. A nonergodic process. J Am Chem Soc 120(13):3265–3266
53. Shvartsburg AA, Smith RD (2008) Fundamentals of traveling wave ion mobility spectrometry. Anal Chem 80(24):9689–9699. doi:10.1021/ac8016295
54. Giles K, Wildgoose JD, Langridge I, Campuzano I (2010) A method for direct measurement of ion mobilities using a travelling wave ion guide. Int J Mass Spectrom 298:10–16
55. Campuzano I, Bush MF, Robinson CV, Beaumont C, Richardson K, Kim H, Kim HI (2012) Structural characterization of drug-like compounds by ion mobility mass spectrometry: comparison of theoretical and experimentally derived nitrogen collision cross sections. Anal Chem 84(2):1026–1033. doi:10.1021/ac202625t